DOE/NV/25946--3086

Mie Scattering Analysis

Preliminary Report

December 13, 2016

Marylesa Howard, Aaron Luttman
Signal Processing and Applied Mathematics
National Security Technologies, LLC
Nevada Operations

Daniel Frayer, Daniel Marks
National Security Technologies, LLC
New Mexico Operations

with contributions from

Martin Schauer
Los Alamos National Laboratory

Paul Steele
Lawrence Livermore National Laboratory

This report was authored by the National Security Technologies, LLC, under Contract No. DE-AC52-06NA25946 with the U.S. Department of Energy.

EXECUTIVE SUMMARY

Mie scattering theory describes how light scatters off a particle cloud when the particle size is approximately the same as the wavelength of scattered light. Assuming the particles generated in an ejecta experiment are spherical, one goal of such experiments is to determine the particle radii distribution, which in theory can be done by measuring intensities of scattered light at several different angles. The purpose of this report is the present an assessment of how closely the analysis of Mie scattering data in practice reflects the theoretical possibilities.

Recommendations: The analysis presented in this report leads to the following recommendations for fielding a Mie scattering diagnostic in dynamic experiments:

- Robust prior estimates for the mean and variance, within 20% of the true values, of the particle radius distribution are required to determine optical diagnostic setup in order for the analysis to give meaningful results. It is better to overestimate the mean.
- At least 12 angles should be selected at which to measure the scattered light intensity.
- The recommended angle placements for the detectors are related to the expected mean and variance of the particle radius distribution, for which we have a formula for their adequate distribution.
- The raw intensity profiles must be measured, calibrated, and analyzed, including transmission data. The data should *not* be peak or area normalized.

Given the results detailed in this report, these recommendations maximize the potential for Mie scattering measurements to yield data that can be effectively analyzed.

Further Studies: To increase the confidence level with which we can obtain meaningful Mie scattering measurements, there are several further topics of study that are required:

- The choice of histogram binning for the distribution of the radius is up to the analyst, but it plays a significantly crucial role in the accuracy of the radius mean and variance estimates. Further study needs to be completed to understand the role the choice in binning the radius distribution plays in reconstruction of experiment data.
- Current literature assumes a lognormal distribution for the particle radius, which is incorporated in the analysis here. Further studies should include non-lognormal distribution assumptions, including the case in which no distributional assumption is made.
- Additional studies should include modeling a finite size detector at each angle (specified angle plus tolerance) to better mimic an experiment setup, as opposed to the current studies that assume a point detector.
- In multi-wavelength extinction, an analogue of multi-angle Mie scattering, our studies suggest the greater number and range of wavelengths emitted, the more precise the estimates of particle radius mean and variance. These two diagnostics can potentially complement each other, and a study of how the two can jointly increase confidence in the analysis should be undertaken.

Table of Contents

1 Introduction

When metals are subjected to intense shock loadings, it is common for particulates to be emitted from the surface of the metal, and, in order to understand the physical processes that govern this release, it is necessary to be able to measure the size distribution of the ejecta particles in situ.

Two diagnostic approaches using Mie scattering theory to estimate particle size distribution have been studied recently: multi-angle Mie scattering and multi-wavelength extinction. The multi-angle diagnostic measures the amount of single-wavelength laser light scattered off the medium at specified angles in addition to measuring transmission – an on-axis measurement of light that is not scattered or absorbed by the medium. Current multi-angle experiments use twelve off-axis angles [7]. Figure 1 provides an illustration and photo of the angle setup for data collection via fiber optics that feed into photomultiplier tubes. The multi-wavelength extinction (MWE) diagnostic measures transmission of laser light composed of multiple wavelengths at a single angle, with recent experiments fielding eight wavelengths [9, 10]. Figure 2 (a) shows the footprint of the MWE diagnostic with a layout of the multi-laser arrangement (b) and a diagram of the setup in-situ during a dynamic experiment (c).

(a)

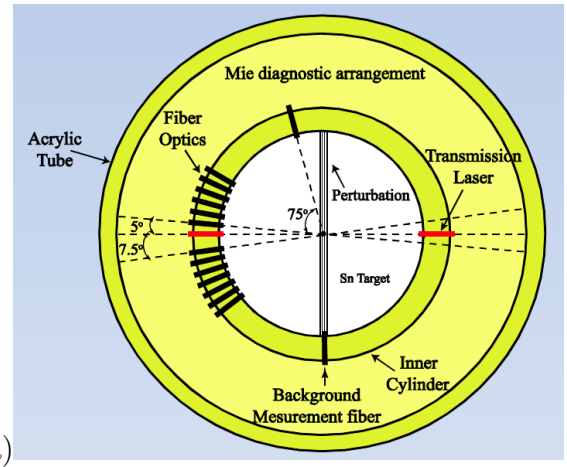

(b)

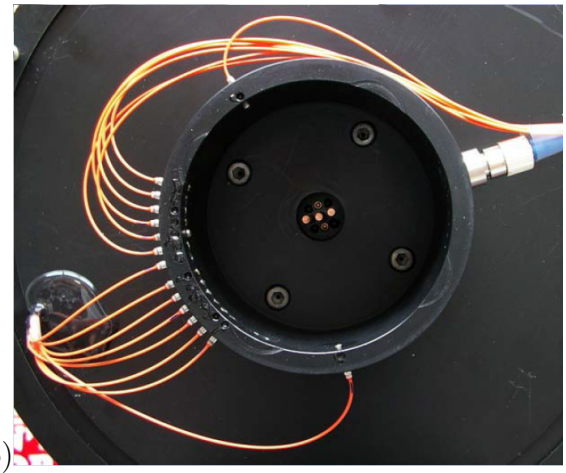

Figure 1: (a) A diagram of the Mie Scattering diagnostic setup as laser light is scattered off an object and detected through fiber optic cabling at specific angles. (b) A picture of an experiment setup where ejecta would be observed in the center of the ring.

In this report, we address specific questions as to what can be determined through analysis of the multi-angle Mie scattering diagnostic data. We discuss the model assumptions, the best results achievable in theory, the effect of the number of angles chosen and the placement of those angles, the effect of the magnitude of radius mean and variance, the effect of noise, and the effect of data normalization. Further studies need to be completed in a similar manner for the multi-wavelength extinction diagnostic.

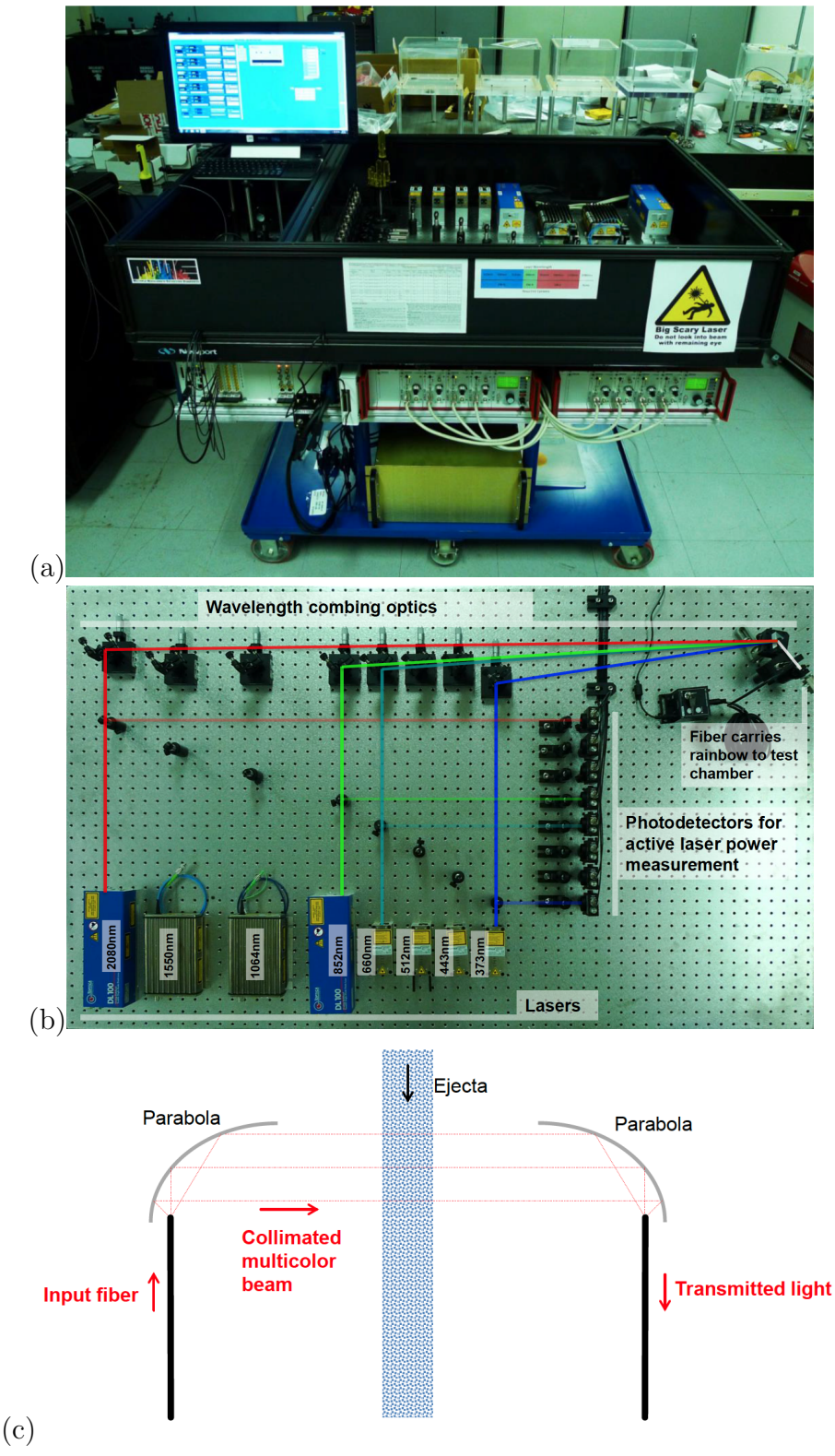

Figure 2: (a) The multi-wavelength extinction diagnostic setup. (b) The arrangement of the multiple wavelengths of interest. (c) A diagram of the diagnostic setup in-situ during a dynamic experiment.

2 Multi-angle Mie scattering

The model describing Mie scattering is presented in its entirety in Appendix A and is derived in [1, 2]. The model describes the intensity of scattered light observed at selected angles θ, given a distribution of particle sizes α, where the radius of the particle is r.

In the remainder of this chapter we lay out some of the basic assumptions that are required for the Mie scattering approach to be viable as well as recommendations for fielding and analyzing these diagnostics.

2.1 Assumptions

Inherent in the model are assumptions requiring spherical particles with radius on the same order of magnitude as the laser light with single scattering of the laser light [1, 2]. The model involves a distribution for α but does not make distributional assumptions, though the statistics of interest are on the radius of the particle r so we determine the relationship between the distributions on α and r.

Mie Scatter Model Assumptions:

- The particles are assumed to be spherical [1, 2].
- The particles are assumed to have radius on the order of magnitude as the wavelength (Mie scattering regime) [1].
- Only single scattering occurs, and no phase relations exist between light scattered from different particles [1].

2.1.1 Lognormal distributions on α and r

The Mie scatter model includes the probability distribution $f(\alpha)$ for the particle size parameter α, which is directly proportional to radius parameter r. In practice, for aerosol particle size distributions, it is suggested in the literature to assume a lognormal distribution [3, 6, 8, 11, 12].

Preliminary Results on the Distributions of α and r:

- The particle size parameter α has a lognormal distribution if and only if the radius r has a lognormal distribution. Both distributions have different, but relatable, parameters.
- The mean of the particle radius is denoted μ and the variance of the particle radius is denoted σ^2, and they are sufficient to describe the lognormal distribution of r.

Future work:

- Further studies should be performed to include non-lognormal distribution assumptions, including the case in which no distributional assumption is made.

We begin by assuming $f(\alpha)$ has a lognormal distribution as currently done in multi-angle Mie scattering and multi-wavelength extinction analysis [7, 10, 9]. The lognormal distribution for α is sufficiently defined by location parameter γ_α and scale parameter δ_α and is given by

$$f(\alpha) = \frac{1}{\alpha\delta_\alpha\sqrt{2\pi}} e^{-\frac{(\ln\alpha-\gamma_\alpha)^2}{2\delta_\alpha^2}}. \tag{1}$$

The real variable of interest in Mie scattering is the radius, r, where

$$r = \frac{\lambda}{2\pi n_m}\alpha, \tag{2}$$

λ is the wavelength of the light and n_m is the refractive index of the medium. We are specifically interested in the mean μ and variance σ^2 of the distribution on r. The particle size parameter α has a lognormal distribution if and only if the particle radius r has a lognormal distribution. Notationally, given $\alpha \sim \text{Lognormal}(\gamma_\alpha, \delta_\alpha)$ and (2), then $r \sim \text{Lognormal}(\gamma_r, \delta_r)$, where $\gamma_r = \gamma_\alpha + \ln\left(\frac{\lambda}{2\pi n_m}\right)$ and $\delta_r = \delta_\alpha$ (see Appendix C for proof). The mean of the distribution on r is given by

$$\begin{aligned} \mu =& e^{\gamma_r+\delta_r^2/2} && \text{(in terms of } r\text{)}, && (3)\\ =& \frac{\lambda}{2\pi n_m} e^{\gamma_\alpha+\delta_\alpha^2/2} && \text{(in terms of } \alpha\text{)}, && (4) \end{aligned}$$

and the variance by

$$\begin{aligned} \sigma^2 =& (e^{\delta_r^2}-1)e^{2\gamma_r+\delta_r^2} && \text{(in terms of } r\text{)}, && (5)\\ =& \left(\frac{\lambda}{2\pi n_m}\right)^2 (e^{\delta_\alpha^2}-1)e^{2\gamma_\alpha+\delta_\alpha^2} && \text{(in terms of } \alpha\text{)}. && (6) \end{aligned}$$

Stating the values μ and σ^2 is sufficient for describing the lognormal distribution of r.

2.2 Reconstructions with noiseless data

It is unrealistic that experiment data will be entirely free from measurement or other kinds of noise; however, we first examine the Mie scatter model without noise to understand the best case scenario in terms of what we can extract from the data. We consider the impact of the number of angles used in the experiment to observe scatter intensity, the placement of those angles, and the effect of the magnitude of the particle radius mean and variance on our ability to reconstruct those parameters.

Table 1: In noiseless data, obtaining measurements for both the positive and negative angle value does not provide additional information beyond what is gained from observations at either the positive or negative angle value but not both. The true values are $\mu = 2.0$ and $\sigma^2 = 2.0$.

θ discretization	$\hat{\mu}$ (% error)	$\hat{\sigma}^2$ (% error)
$\{1, 2, 3, 4, 5\}$	1.9997 (0.02)	1.9980 (0.1)
$\{-4, -2, 1, 3, 5\}$	1.9997 (0.02)	1.9980 (0.1)
$\{-5, -4, -3, -2, -1, 1, 2, 3, 4, 5\}$	1.9997 (0.02)	1.9980 (0.1)

Preliminary Results on Theoretical Reconstructions:

- The decay of the light intensity, $I(\theta)$, is directly related to the radius distribution mean μ and variance σ^2, and it is essential to distribute the detectors at angles throughout the peak and tails of the expected light intensity profile.
  - Formulas for determining detector angles are given in the text below.
  - This requires having initial estimates of μ and σ^2 prior to the diagnostic setup.
  - Generally, the smaller the prior estimates of μ and σ^2, the more flexibility we have in choosing the angle placement.
- In the no-noise case, reconstructions tend to overestimate the mean particle radius when there are no small angle detectors.

Future work:

- Further studies should include a finite size detector at each angle (specified angle plus tolerance) to better mimic an experiment setup.

2.2.1 The effect of the number of angles

The Mie scatter intensity profile $I(\theta)$ is symmetric and unimodal about the transmission angle (0 degrees)When no noise is present in the data, there is no additional information in the data when a negatively-valued angle is observed in conjunction with the same-valued positive angle. This is observed in Table 1 where five angle values are chosen (integers 1 through 5), but negating the angles or including observations at both positive and negative angles provides no additional power in our ability to reconstruct the mean and variance of r. The same does not hold true in data with noise.

2.2.2 The effect of angle placement

The decay of the scatter intensity profile $I(\theta)$ depends on the parameters of the lognormal distribution on r, which affects optimal angle placement. Given estimates of μ and σ^2 prior

Table 2: In noiseless data, the choice of angle values has drastic effect on our ability to accurately reconstruct parameters of interest and is influenced by the values μ and σ^2. The true values are $\mu = 2.0$ and $\sigma^2 = 2.0$.

θ discretization	$\hat{\mu}$ (error)	$\hat{\sigma}^2$ (error)
$\{-5, -4, -3, -2, -1, 1, 2, 3, 4, 5\}$	1.9997 (0.02%)	1.9980 (0.1%)
$\{-1, -0.8, -0.6, -0.4, -0.2, 0.1, 0.3, 0.5, 0.7, 0.9\}$	2.0006 (0.03%)	1.9956 (0.22%)
$\{-45, -40, -35, -30, -5, 4, 28, 33, 38, 43\}$	1.9891 (0.55%)	1.8769 (6.2%)
$\{-45, -40, -35, -30, -5, 12, 28, 33, 38, 43\}$	1.9887 (0.57%)	1.8982 (5.1%)
$\{-45, -40, -35, -30, -10, 12, 28, 33, 38, 43\}$	1.9727 (1.4%)	2.4329 (21.6%)
$\{2, 30, 32, 34, 36, 38, 40, 42, 44, 46\}$	140 ($> 100\%$)	9e7 ($> 100\%$)

to the experiment, we can compute the angles ranges that correspond to the peak of the intensity profile, such as the full-width 5% and 1% maximums, noted FW5M and FW1M, respectively. For select μ and σ^2, we have computed the absolute value of the associated angles in Appendix D. We recommend placing at least two detectors within the FW5M range, at least two detectors between the FW5M and FW1M ranges, and at least four detectors outside of the FW1M range.

To disentangle the effect of the number of angles with angle placement, the number of angles was set to ten, with $\mu = 2.0$ and $\sigma^2 = 2.0$; note the FW5M is $(-5.14°, 5.14°)$ and the FW1M is $(-12.89°, 12.89°)$. Table 2 shows the effect of angle placement on reconstruction error of $\hat{\mu}$ and $\hat{\sigma}^2$ given different sets of observation angles. The first set of angles in the table is entirely within the FW5M and produces the least error of those sets. The second set of angles has a narrower span of θ and produces estimates with slightly higher error, indicating predictive power in having observations distributed evenly within the FW5M range. The remaining three sets have many of the angles in the tails, with some values in the FW5M or FW1M range. We observe that having at least two angles within the FW1M greatly reduces estimate error, where a conservative approach ensures that at least one of the angle observations is within the FW5M. Thus, to choose angles appropriately, we first need an estimate of μ and σ^2 for the experiment in order to determine the θ range of the FW5M/FW1M. When the angles observed in the experiment are entirely contained in the tails of that profile (outside the FW1M range), the predictive power of the data goes down. Even distribution of angles in the FW5M/FW1M range produces the greatest reduction in reconstruction error.

2.2.3 The effect of magnitude of mean and variance of particle radius

As described above, the values of μ and σ^2 affect the decay of the Mie scatter intensity, and therefore, affect which angles fall within, for example, the FW1M. Most generally, the smaller the mean and variance of the particle radius, the wider the range of the FW1M. For example, if $\sigma^2 = 2.0$ but we increase μ from 2.0 to 10.0, the range of the FW5M is reduced from $(-5.14°, 5.14°)$ to $(-1.89°, 1.89°)$, restricting the range of angles to choose from to ensure at least two fall within the range of the FW5M. Thus, larger particle sizes

Table 3: The magnitude of the particle radius mean affects the decay of the Mie scatter intensity profile, affecting the range of the FW1M, and, therefore, the angles that should be observed. Here, $\sigma^2 = 2.0$ while the mean particle radius is observed at 2.0 and 10.0 microns and reconstruction error is obtained for two different sets of angle observations in the no-noise scenario.

$\theta = \{1, 2, 3, 4, 5\}$	$\hat{\mu}$ error	$\hat{\sigma}^2$ error	Description of θ distribution
$\mu = 2.0$	0.02%	0.10%	θ entirely within FW5M
$\mu = 10.0$	$< 0.01\%$	0.82%	θ distributed throughout FW5M, FW1M, and tails
$\theta = \{-15, -7, -3, 4, 9\}$	$\hat{\mu}$ error	$\hat{\sigma}^2$ error	Description of θ distribution
$\mu = 2.0$	0.18%	4.59%	θ distributed throughout FW5M, FW1M, and tails
$\mu = 10.0$	50.13%	49.71%	no θ within FW5M or FW1M

typically restrict our available θ choices to a smaller range of angles. Table 3 demonstrates the increased estimate error when the mean particle size increases for a given set of observed angles that falls outside of the FW5M.

2.3 Reconstructions with noisy data

Realistically, we expect noise in our data from the measurement system. The analysis of noiseless data above allows us to measure the extent to what we can say about the data simply through the model itself. Noise almost certainly always adds an additional layer of error in the reconstructions, and the extent of its effects are described here.

Preliminary Results on Reconstructions from Noisy Data:

- Increasing the number of angles observed within an interval leads to less variation in the estimates of μ and σ^2 due to noise.
  - Additional angles serve to stabilize the estimates and reduce variation in the reconstructions due to noise.
- Twelve angles that are appropriately distributed in θ minimizes variation in data estimates due to noise while accounting for space constraints in the diagnostic.
  - More than twelve angles reduces variation but with diminishing returns.
  - At 10% added error, $\hat{\mu}$ will typically be within 12% of the truth and $\hat{\sigma}^2$ will typically be within 70% of the truth. With half that noise, these errors are reduced by about half.
- Raw intensity provides significantly more predictive power over normalizing the data.
  - Detector calibrations to true intensity are essential to maintaining raw data.

Future work:

- Study the nonlinear-relationship between the estimate pair $(\hat{\mu}, \hat{\sigma}^2)$ and what this indicates about uncertainty.

2.3.1 The effect of the number of angles

To test the effect of the number of angles, we observed 200 realizations of intensity data with $\mu = 2.0$, $\sigma^2 = 2.0$, and 10% noise for n linearly spaced angles between -21° and 20°, where $n = 2, \ldots, 100$. The angle interval choice serves to ensure no angles are duplicated at the positive/negative values. The relative percent variations of middle 95^{th} percentiles of $\hat{\mu}$ and $\hat{\sigma}^2$ are given in Figure 3 (a) and (b), respectively, as a function of the number of θ. Fewer than twelve angles can lead to significantly higher variation in $\hat{\mu}$ and $\hat{\sigma}^2$. Considering the data measured at twelve angles, 95% of the time $\hat{\mu}$ will be within 12% of the truth and $\hat{\sigma}^2$ will be within 70% of the truth.

2.3.2 The effect of noise magnitude

In Section 2.3.1, we considered the reconstruction error associated with twelve angles and 10% added noise. Similarly, when we compute the same statistics for data observed at twelve angles with $\mu = 2.0$, $\sigma^2 = 2.0$, and 5% added noise, 95% of the time the reconstruction of μ will be within 5.5% of the truth and the reconstruction of σ^2 will be within 24% of the truth. If the experiment were repeated many times, the average reconstruction of μ would be off by 0.07% and the average reconstruction of σ^2 would be off by 2.6%. Reducing the noise by 50% reduces the reconstruction error for $\hat{\mu}$ by approximately half and the reconstruction error of $\hat{\sigma}^2$ by more than half.

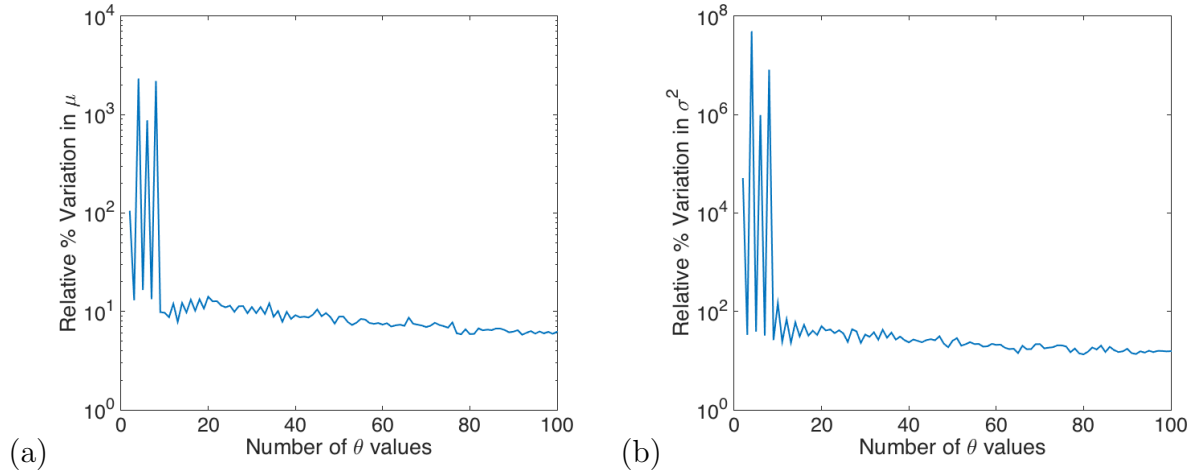

Figure 3: Two hundred data sets were generated with 10% added noise, $\mu = 2.0$, and $\sigma^2 = 2.0$ for n linearly spaced angles between $-21°$ and $20°$, where $n = 2, \ldots, 100$. The relative percent variation from 95^{th} percentiles are shown for $\hat{\mu}$ (a) and $\hat{\sigma}^2$ (b).

2.3.3 The effect of normalizing data

If the raw scatter intensities or detector calibrations are unknown, it may be tempting to normalize the data observations across the angles at any point in time. The scale of intensity in the data provides significant reduction in uncertainty for $\hat{\mu}$ and $\hat{\sigma}^2$. We visualize this change in uncertainty with a parameter search map: we consider a wide range of μ and σ^2 pairs and compute the corresponding Mie scatter intensity profile to which we compare the data by computing

$$e^{-\frac{1}{2s^2}||\mathbf{b}-\mathbf{f}(\mu_i,\sigma_i^2)||^2}, \tag{7}$$

where $\mathbf{b}$ is the data vector, $\mathbf{f}(\mu_i, \sigma_i^2)$ is the corresponding scatter intensity model for radius distribution parameters μ_i and σ_i^2, and s is the known error in the data.

Figure 4 images the values of (7) for a given data set with an added 10% noise realization (a) and the corresponding best fit to the data is given in (b), where $\hat{\mu} = 2.09$ and $\hat{\sigma}^2 = 2.27$. When the data are normalized, the corresponding parameter search map is given in (c) with best fit to the normalized data in (d) and estimates $\hat{\mu} = 2.36$ and $\hat{\sigma}^2 = 2.34$. The estimates for the non-normalized data are closer to the truth, perhaps not too significantly, but the uncertainty in the estimates for the normalized data are large in both μ and σ^2 because there are many (μ, σ^2) pairs that provide similar fits to the normalized data (c). With raw data, there is some uncertainty in σ^2, but much less uncertainty in μ, as seen in (a). In both cases, the curved shape of the parameter search maps indicate a relationship between the best fit pair (μ, σ^2), which should be explored further.

2.4 Discretization of the radius

The discrete Mie model is given in (17), and it involves a discretization in both θ and r, the latter of which plays a significantly crucial role in the accuracy of the estimates. The θ

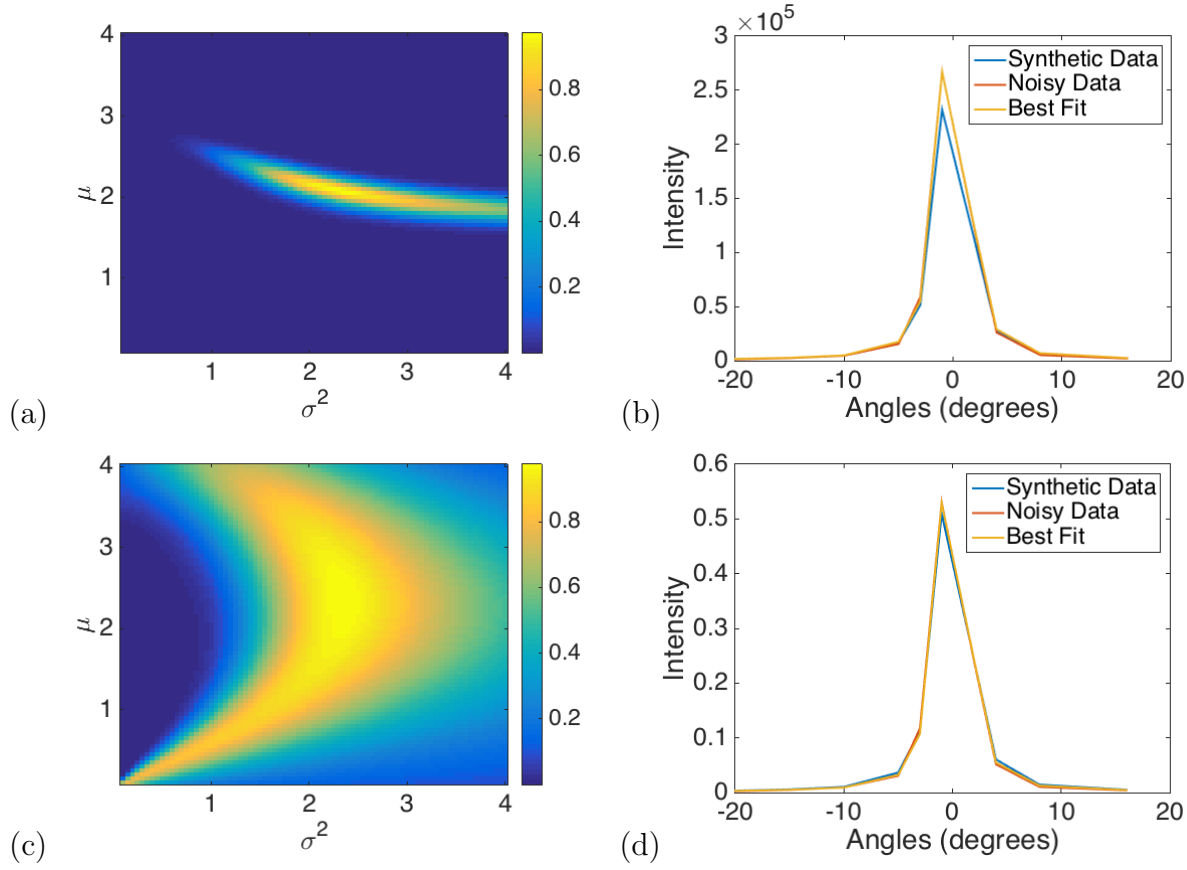

Figure 4: Given a data set with a realization of 10% added noise, the corresponding parameter search map is given in (a) and best fit to the data is given in (b), with estimates $\hat{\mu} = 2.09$ and $\hat{\sigma}^2 = 2.27$. When the data are normalized and refit to the model, the resulting parameter search map is given in (c) and best fit to the data is given in (d), with estimates $\hat{\mu} = 2.36$ and $\hat{\sigma}^2 = 2.34$. Estimates are more accurate when the data are *not* normalized. The yellow indicates parameter pairs that fit the data well, and there is much more uncertainty in μ when the data are normalized (c).

discretization is directly related to the experiment, because the discrete θ values correspond to the angles at which the detectors are placed. The data do not dictate the discretization of r, as they do with θ, and the choice of increment and range of values (choice of binning) provides a baseline error in the parameter reconstructions that cannot be overcome in the analysis via other parameters, e.g. changing the number of angles.

Preliminary Results on the Discretization of r:

- The discretization of particle radius r chosen by the analyst directly affects the quality of the reconstruction.
- To minimize reconstruction error, choose the histogram interval for r from near 0 to 10 microns, and choose binning widths of no less than 0.2 microns.
- All further statements in this report about reconstruction error are predicated on the assumption that we have minimal error due to a poor or inaccurate discretization in r.

Future work:

- As r is not discretized in the generation of experiment data, further study needs to be done to understand the role the discretization of r plays in reconstruction of experiment data.

Given data observations of intensity, we automatically know the discretization of θ used to generate or observe the data, and therefore we use that same discretization to reconstruct the mean μ and variance σ^2 that describe the particle radius distribution. The discretization of r, which is not a component of the observed data, is also required to invert the model computationally, and its choice is left to the analyst.

In the generation of synthetic data, the discretization of r is known thus it may be tempting to use the same discretization to reconstruct parameters describing the distribution of r. This is known as an *inverse crime*, the act of using the same model to both generate and invert the data. Here, we determine the effect of using an r discretization for reconstruction that is different than the discretization used to generate synthetic data.

An example of synthetic data is given in Figure 5, where we observe the intensity at angles between -10° and 10° in half degree increments and bin the r values from 0.1 to 5.0 microns in increments of 0.1 microns. No noise is added, and we let $\mu = 2.0$ microns, $\sigma^2 = 2.0$ microns, $\lambda = 0.638$ microns, $n_m = 1$, and the refractive index of the particle be 1.2.

Given the data observations, we invert the Mie scatter model to obtain estimates for the mean and variance of the particle radius distribution, $\hat{\mu}$ and $\hat{\sigma}^2$, respectively. Using six different discretizations of r, including the discretization used to generate the data, we reconstruct the parameters of interest in the first half of Table 4 for the noiseless data presented in Figure 5. We repeat this process for data generated using the r discretization of values between 0.1 and 10.0 in increments of 0.1. The noiseless data case, while unrealistic for real data, provides a baseline error for us to understand the effect of the r discretization.

The results in the table suggest that knowing the exact model used to generate the data is truly the best case scenario, but, in practice, that is unreasonable to expect because r is

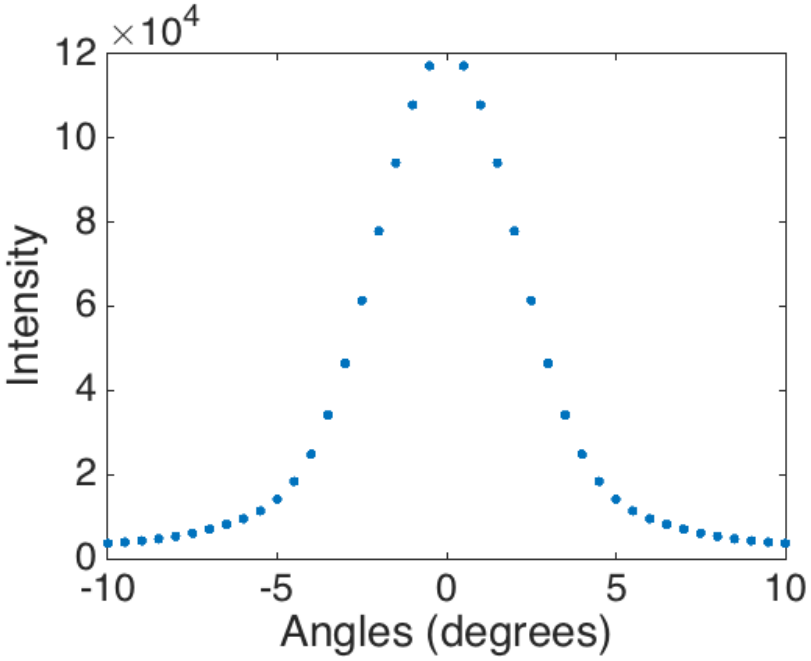

Figure 5: Synthetic intensity data without noise where θ ranges from $-10°$ and $10°$ in half degree increments and the r discretization takes on values from 0.1 to 5.0 microns in increments of 0.1 microns.

Table 4: Given the data presented in Figure 5, estimates for μ and σ^2, denoted $\hat{\mu}$ and $\hat{\sigma}^2$, respectively, were computed with the different r generation and reconstruction discretizations noted below. The true values are $\mu = 2.0$ and $\sigma^2 = 2.0$.

r discretization for generation	r discretization for reconstruction	$\hat{\mu}$	$\hat{\sigma}^2$	Relationship to original discretization
$\{0.1, 0.2, \ldots, 5.0\}$	$\{0.125, 0.175, \ldots, 4.975\}$	2.0217	2.1543	More densely sampled
	$\{0.15, 0.25, \ldots, 4.95\}$	2.0226	2.1665	Same spacing
	$\{0.15, 0.35, \ldots, 4.95\}$	2.0014	2.0237	More sparsely sampled
	$\{0.15, 0.25, \ldots, 9.95\}$	1.9164	0.7720	Larger span; same spacing
	$\{0.15, 0.35, \ldots, 9.95\}$	1.9165	0.7718	Larger span; sparsely sampled
	$\{0.1, 0.2, \ldots, 5.0\}$	2.0000	2.0000	Inverse Crime
$\{0.1, 0.2, \ldots, 10.0\}$	$\{0.125, 0.175, \ldots, 9.975\}$	1.9990	2.0097	More densely sampled
	$\{0.15, 0.25, \ldots, 9.95\}$	1.9990	2.0078	Same spacing
	$\{0.15, 0.35, \ldots, 9.95\}$	1.9999	1.9974	Sparsely sampled
	$\{0.15, 0.25, \ldots, 4.95\}$	5.4387	0.2667	Smaller span
	$\{0.15, 0.35, \ldots, 4.95\}$	5.6065	0.4366	Smaller span
	$\{0.1, 0.2, \ldots, 10.0\}$	2.0000	2.0000	Inverse Crime

not discretized to generate the experiment data. In the cases where the r discretization for reconstruction is different from that used to generate the data, we observe that it is better to overestimate the span of the interval of r values rather than underestimate, though it is best to use the same span when known. Furthermore, there may be slight improvement in discretizing at sparser spacing increments than selecting more densely sampled discretizations.

Based on these observations, aiming to avoid committing an inverse crime, and maintaining a "best case scenario" for the discretization of r, the synthetic data used above in this report was generated using the discretization $r \in \{0.1, 0.2, \ldots, 10.0\}$ and reconstructed using the discretization $r \in \{0.15, 0.35, \ldots, 10.0\}$. All statements about reconstruction error are predicated on the assumption that we have minimal error due to a poor or inaccurate discretization in r.

3 Multi-wavelength extinction

Mie theory also allows information about particle size distributions to be extracted from the scattering and transmission of light from multiple wavelengths. We will first consider the case where only transmission information is used and then consider the case in which scattering data is also observed. We make the same assumptions about the particle distribution and shape as above.

Preliminary Results on MWE:

- Analysis using transmission data is extremely sensitive to system calibrations.
- Low transmission provides better analysis and its is not affected by multiple scattering.
- The greater the number and range of wavelengths emitted, the more precise the determination of the distribution parameters μ and σ^2.

Future work:

- Further analysis of simulation results to determine a recommended wavelength set.

3.1 Reconstruction from transmission data with multiple wavelengths

Unlike the Mie scattering reconstructions, the use of transmission data is much more sensitive to the precise calibrations of the optical and detection system. With Mie scattering, any factor that uniformly reduces the light level on all detectors will lead to an error in the estimate of the particle concentration but will not produce an error in the distribution parameters μ and σ^2. In the case of transmission data, errors in the laser intensity and detector sensitivity can be calibrated using the transmission data from before the experiment begins.

Table 5: Errors in the estimates for μ and σ^2 averaged over 100 simulations. The true distribution values are $\mu = 2.0$ and $\sigma^2 = 2.0$ for a wavelength of 1000 nm. Maximum transmission for all simulations was 10%, meaning that the largest signal from all wavelengths was 10% of the unobstructed signal, before the addition of 5% noise.

Wavelengths Used (nm)	$\hat{\mu}$ error	$\hat{\sigma}^2$ error
$\{800, 900, 1000, 1100, 1200\}$	75%	$\geq 100\%$
$\{500, 750, 1000, 1250, 1500\}$	26%	$\geq 100\%$
$\{500, 700, 900, 1100, 1300, 1500\}$	16%	78%
$\{500, 600, 700, 800, 900, 1000,$ $1100, 1200, 1300, 1400, 1500\}$	75%	48%

Other errors that affect light transmission, such as errors in the absorption component of the complex index of refraction, will greatly affect the results from transmission data.

3.1.1 Reconstruction from transmission data alone

We simulated the results of using only transmission data for 11 wavelengths from 500 nm to 1500 nm spaced in 100 nm steps, as well as smaller sets of wavelengths. We assumed no errors in the calibration of the system, but did add 5% noise. We used values of $\mu = 2.0$ and $\sigma^2 = 2.0$ for the true particle distribution for 1000 nm wavelength. Since μ and σ^2 depend on wavelength, a single wavelength had to be chosen to define the distribution. Unlike the Mie scattering data, there is no problem if there is multiple scattering. In fact, the transmission data gives better results if the transmission is low. We used a maximum transmission value of 10% for all of these simulations. Results are given in Table 5.

We see that for transmission data it is not only the number of wavelengths used that matters, but the range of wavelengths is also important. When the full range from 500 nm to 1500 nm is used, the addition of more wavelengths within this range reduces the uncertainty in μ and σ^2, but we have seen a similar effect by simply reducing the noise. The significance of more wavelengths seems to be the additional sampling that reduces the effects of noise, rather than the additional information from the wavelengths themselves. If noise is reduced to zero and transmission is also decreased, the reconstructions are much better, but we wanted to demonstrate the limits of multi-wavelength extinction with realistic noise. A greater range of wavelengths would also give better results, but would also be more difficult to field.

3.1.2 Reconstruction from transmission and scattering data

The use of information from both transmission and scattering data turns out to provide significantly better results than either diagnostic used alone. To make the system simpler we assumed that a wavelength of 638nm would used for both scattering and transmission. Obviously the addition of other wavelengths for both transmission and scattering data would provide more information and improve the reconstructions, but the single wavelength system

Table 6: Errors in the estimates for μ and σ^2 averaged over 100 simulations for scattering and transmission data combined. The true distribution values are $\mu = 2.0$and $\sigma^2 = 2.0$ and the wavelength used was 638nm. Maximum transmission for all simulations was 66% and the simulated data had 5% noise added. Scattering data had 10 angles spaced evenly from 2.5° to 25°.

Simulation	μ error	σ^2 error
Scattering data alone	24%	87%
Scattering data and transmission data	7%	33%

shows the benefits of this combination clearly. We used scattering data from 10 angles $(2.5°, 5.0°, 7.5°, 10.0°, 12.5°, 15.0°, 17.5°, 20.0°, 22.5°, 25°)$ and transmission data from a single detector at 0°. The transmission at the 0° detector was 66%, enough to minimize the effects of multiple scattering. The noise level was set to 5% for both the scattering and transmission data. As before, the distribution parameters were set to $\mu = 2.0$ and $\sigma^2 = 2.0$. Results are given in Table 6.

The addition of a single detector at 0° provides a substantial reduction in the uncertainty of the distribution parameters, largely due to the fact that the transmission measurement narrows the uncertainty in the particle concentration. We have only reported uncertainties in μ and σ^2 in this report, but particle concentration is the third variable which indirectly affects the estimates of μ and σ^2. If the particle concentration is known exactly, the estimates of μ and σ^2 are automatically improved. We find that a single value of transmission for one wavelength does a good job of narrowing the estimates of particle concentration since the transmission is relatively insensitive to the values of μ and σ^2.

As was pointed out at the beginning of the previous section, the use of transmission data requires that the system be well calibrated. Anything unforeseen that produces a uniform drop in signal will greatly reduce the value of the transmission data. This applies as well for the combined scattering and transmission data. If there were some absorption of light in the particle cloud unaccounted for by our scattering model, the scattering data would still be useful as long as this unforeseen effect didn't affect the relative scattering. Absorption that is unaccounted for in our model could render the transmission data almost useless.

Appendix A: Mie Model

Mie scattering describes the light scatter from particles of radius comparable to the wavelength of light scattering off the particles while Rayleigh scattering describes light scattering from particles of radius much smaller than the wavelength of light; the third case, particle of radius much larger than the wavelength of light, is described by the Fraunhofer diffraction limit [1]. Mie theory, developed by Gustav Mie in 1908 [4], Maxwell's equations may be solved to describe the incident, scattered, and internal fields of an electromagnetic wave on spherical particles with appropriate boundary conditions [5], and, in particular for the Fraunhofer limit, the theory is derived correctly for small angles in the forward direction where $\sin(\theta) \approx \theta$ [1]. More specifically, the Fraunhofer region is applicable for radii greater than about ten times the wavelength of light, and the scattered intensity $I_s(\theta)$ per unit area of detector is given by

$$I_s(\theta) = I_i \int_{\alpha_0}^{\alpha_1} |S(\theta, \alpha)|^2 f(\alpha) d\alpha \tag{8}$$

where I_i is the total transmission, $S(\theta, \alpha)$ is the scattering function, and $f(\alpha)$ is a continuous probability distribution for the particle size parameter α [1, 2]. The particle size parameter is given by

$$\alpha = \frac{2\pi n_m}{\lambda} r, \tag{9}$$

where n_m is the refractive index of the medium, λ is the wavelength, and r is the particle radius. In experiments and simulations presented here, $\lambda = 0.638$ μm. For both vacuum and helium, we take $n_m = 1$. For simulations, we let the refractive index of the particle $n_p = 1.2$, and for experiments with tin the complex refractive index of the particle is $n_p = 2.2 + 5.4i$.

From Bohren and Huffman, the components of the scattering function can be written as [2]

$$|S(\theta, \alpha)|^2 = \sqrt{||S_1(\theta, \alpha)||^2 + ||S_2(\theta, \alpha)||^2}, \tag{10}$$

where

$$S_1(\theta, \alpha) = \sum_{k=1}^{\infty} \frac{2k+1}{k(k+1)} \left(a_k(\alpha) \pi_k(\theta) + b_k(\alpha) \tau_k(\theta) \right), \tag{11}$$

$$S_2(\theta, \alpha) = \sum_{k=1}^{\infty} \frac{2k+1}{k(k+1)} \left(a_k(\alpha) \tau_k(\theta) + b_k(\alpha) \pi_k(\theta) \right), \tag{12}$$

with Mie scatter coefficients $a_k(\alpha)$ and $b_k(\alpha)$ given by

$$a_k(\alpha) = \frac{\nu \psi_k(\nu\alpha) \psi_k'(\alpha) - \psi_k(\alpha) \psi_k'(\nu\alpha)}{\nu \psi_k(\nu\alpha) \xi_k'(\alpha) - \xi_k(\alpha) \psi_k'(\nu\alpha)}, \tag{13}$$

and

$$b_k(\alpha) = \frac{\psi_k(\nu\alpha) \psi_k'(\alpha) - \nu \psi_k(\alpha) \psi_k'(\nu\alpha)}{\psi_k(\nu\alpha) \xi_k'(\alpha) - \nu \xi_k(\alpha) \psi_k'(\nu\alpha)}, \tag{14}$$

where the ratio of the relative refractive index of particle and medium is given by $\nu = n_p / n_m$ [1, 2]. The Mie scatter coefficients are related to $j_k(x)$, the spherical Bessel function of order

n, and $h_k^{(1)}(x)$, the spherical Bessel function of the third kind, also known as the spherical Hankel function, by

$$\psi_k(x) = x j_k(x) \tag{15}$$

and

$$\xi_k(x) = x h_k^{(1)}(x). \tag{16}$$

Further description of the Bessel functions and useful derivative relationships are given in Appendix B.

Discretized Mie Model

Given $\alpha \sim$Lognormal$(\gamma_\alpha, \delta_\alpha)$, we discretize (8) as

$$I_s(\theta_k) = \sum_{j=1}^{J} \frac{I_i}{r_j \delta_\alpha \sqrt{2\pi}} \left| S\left(\theta_k, \tfrac{2\pi n_m r_j}{\lambda}\right) \right|^2 e^{-[\ln(r_j) - (\gamma_\alpha - \ln(2\pi n_m/\lambda))]^2} \Delta r_j, \tag{17}$$

where $\{\theta_k\}$ is the collection of angles at which we took measurements, for $k = 1, \ldots, K$, $\{I_s(\theta_k)\}$ is the collection of calibrated measurements in each angle θ_k, and r_j is our discretization of the radius, for $j = 1, \ldots, J$.

The discretized model in (17) can be simplified to the expression

$$\mathbf{b} = A\mathbf{x}, \tag{18}$$

where a stochastic component may be included to additionally model system noise. In our case, the data $\mathbf{b}$ are the calibrated intensities recorded at the PMTs, adjusted per calibration measurements, for a given point in time. We solve for $\mathbf{x}$, the frequencies of particles with given radii, where $\mathbf{x}$ and $\mathbf{b}$ are related through the Mie scatter model in (8), discretized here as A.

Appendix B: Bessel functions

The spherical Bessel function of the first kind is given by

$$j_k(x) = \sqrt{\frac{\pi}{2x}} J_{k+0.5}(x), \tag{19}$$

where J is the Bessel function of the first kind. The spherical Bessel of the second kind is given by

$$y_k(x) = \sqrt{\frac{\pi}{2x}} Y_{k+0.5}(x), \tag{20}$$

where Y is the Bessel function of the second kind. The spherical Hankel function of the first kind is a linear combination of the first two kinds, given by

$$h_k^{(1)}(x) = j_k(x) + iy_k(x). \tag{21}$$

The derivatives of the spherical Bessel functions are given by

$$[xj_k(x)]' = xj_{k-1}(x) - kj_k(x) \tag{22}$$

and

$$[xh_k^{(1)}(x)]' = xh_{k-1}^{(1)}(x) - kh_k^{(1)}(x). \tag{23}$$

Appendix C: Lognormal distribution theorem

Theorem: Given α $\sim$Lognormal$(\gamma_\alpha, \delta_\alpha)$ and (9), then r $\sim$Lognormal(γ_r, δ_r), where $\gamma_r = \gamma_\alpha + \ln\left(\frac{\lambda}{2\pi n_m}\right)$ and $\delta_r = \delta_\alpha$.

Proof: By definition of a Lognormal distribution, $\ln(\alpha) = \beta \sim$Normal$(\gamma_\alpha, \delta_\alpha)$. Then

$$\begin{aligned}
\ln(r) &= \ln\left(\tfrac{\lambda}{2\pi n_m}\alpha\right), \\
&= \ln(\alpha) + \ln\left(\tfrac{\lambda}{2\pi n_m}\right), \\
&= \beta + \ln\left(\tfrac{\lambda}{2\pi n_m}\right), \\
&\sim \text{Normal}\left(\gamma_\alpha + \ln\left(\tfrac{\lambda}{2\pi n_m}\right), \delta_\alpha\right).
\end{aligned}$$

Since $\ln(r)$ $\sim$Normal$\left(\gamma_\alpha + \ln\left(\frac{\lambda}{2\pi n_m}\right), \delta_\alpha\right)$, then r $\sim$Lognormal(γ_r, δ_r), where $\gamma_r = \gamma_\alpha + \ln\left(\frac{\lambda}{2\pi n_m}\right)$ and $\delta_r = \delta_\alpha$.

Appendix D: Full-width, percent maximum tables

The absolute value x of the angle pair, in degrees, associated with the θ range of the full-width, 5% maximum (FW5M) and full-width, 1% maximum (FW1M) are given in Tables 7 and 8, respectively, where the angle range is given by $(-x, x)$. For example, given $\mu = 2.0$ and $\sigma = 6.0$, the FW5M is contained within the interval $(-3.86, 3.86)$. For example, given $\mu = 5.0$ and $\sigma = 2.0$, the FW1M is contained within the interval $(-7.55, 7.55)$.

Table 7: Absolute value of the angle pair (in degrees) associated with the range of the full-width, 5% maximum of the Mie scatter intensity for a given μ and σ of the r distribution.

		σ									
		1	2	3	4	5	6	7	8	9	10
μ	1	6.53	4.69	4.22	4.01	3.89	3.82	3.76	3.72	3.69	3.66
	2	6.77	5.14	4.47	4.15	3.98	3.86	3.78	3.72	3.68	3.64
	3	5.38	4.61	4.19	3.96	3.81	3.72	3.65	3.60	3.56	3.52
	4	4.13	3.88	3.69	3.57	3.49	3.43	3.39	3.36	3.33	3.31
	5	3.34	3.24	3.17	3.12	3.10	3.08	3.06	3.05	3.05	3.04
	6	2.80	2.75	2.73	2.73	2.73	2.73	2.74	2.74	2.75	2.75
	7	2.41	2.40	2.41	2.43	2.44	2.46	2.47	2.49	2.50	2.52
	8	2.14	2.16	2.19	2.22	2.24	2.26	2.28	2.30	2.32	2.33
	9	1.95	2.00	2.04	2.07	2.10	2.12	2.14	2.16	2.18	2.20
	10	1.84	1.89	1.93	1.96	1.99	2.02	2.04	2.06	2.07	2.09

Table 8: Absolute value of the angle pair (in degrees) associated with the range of the full-width, 1% maximum of the Mie scatter intensity for a given μ and σ of the r distribution.

		σ									
		1	2	3	4	5	6	7	8	9	10
μ	1	17.08	12.58	11.43	10.61	10.10	9.82	9.63	9.49	9.39	9.30
	2	17.94	12.89	11.45	10.46	9.87	9.55	9.34	9.17	9.05	8.94
	3	14.69	11.63	10.13	9.36	8.97	8.69	8.48	8.31	8.19	8.09
	4	11.84	9.82	8.68	8.06	7.73	7.55	7.43	7.36	7.31	7.27
	5	8.32	7.55	7.09	6.85	6.70	6.62	6.57	6.54	6.52	6.51
	6	6.29	6.08	5.90	5.81	5.76	5.74	5.74	5.74	5.75	5.77
	7	5.11	5.04	5.00	4.98	4.98	5.00	5.03	5.06	5.10	5.14
	8	4.34	4.34	4.35	4.36	4.37	4.39	4.42	4.44	4.47	4.50
	9	2.36	4.01	4.05	4.09	4.12	4.14	4.16	4.19	4.21	4.23
	10	2.17	2.29	3.89	3.93	3.97	3.99	4.02	4.04	4.06	4.08

References

[1] S. Arridge, P. van der Zee, D. T. Delpy, and M. Cope. Particle sizing in the mie scattering region: Singular-value analysis. *Inverse Probl.*, 5:671–689, 1989.

[2] C. F. Bohren and D. R. Huffman. *Absorption and Scattering of Light by Small Particles*. John Wiley & Sons, New York, 1983.

[3] O. Boucher, S. E. Schwartz, T. P. Ackerman, T. L. Anderson, B. Bergstrom, B. Bonnel, P. Chylek, A. Dahlback, Y. Fouquart, Q. Fu, R. N. Halthore, J. M. Haywood, T. Iversen, S. Kato, S. Kinne, A. Kirkevag, K. R. Knapp, A. Lacis, I. Laszlo, M. I. Mishchenko, S. Nemesure, V. Ramaswamy, D. L. Roberts, P. Russell, M. E. Schlesinger, G. L. Stephens, R. Wagener, M. Wang, J. Wong, and F. Yang. Intercomparison of models representing direct shortwave radiative forcing by sulfate aerosols. *J. Geophys. Res.*, 103(D14):16979–16998, 1998.

[4] G. Mie. Beiträge zur optik trüber medien, speziell kolloidaler metallösungen [contributions to the optics of turbid media, particularly of colloidal metal solutions]. *Ann. Phys.*, 25(3):377 – 445, 1908.

[5] Michael I. Mishchenko. Maxwell's equations, radiative transfer, and coherent backscattering: a general perspective. *J. Quant. Spectrosc. Radiat. Transfer*, 101(3):540–555, 2006.

[6] Lorraine A. Remer and Yoram J. Kaufman. Dynamic aerosol model: Urban/industrial aerosol. *J. Geophys. Res.*, 103(D12):13859–13871, 1998.

[7] M. Schauer, W. Buttler, S. Monfared, D. Frayer, G. Stevens, and B. La Lone. Dynamic mie scattering experiments. Unpublished presentation; LAUR-13-27058, September 2013.

[8] John H. Seinfeld and Spyros N. Pandis. *Atmospheric Chemistry and Physics: From Air Pollution to Climate Change*. John Wiley & Sons, New York, 1998.

[9] Paul Steele, Steve Compton, Barry Jacoby, and Jose Sinibaldi. The development of new & old ejecta diagnostics at LLNL. Unpublished presentation; LLNL-PRES-680481, November 2015.

[10] Paul Steele, Natalie Kostinski, Steve Compton, and Jose Sinibaldi. Recent developments on a multi-wavelength mie scattering ejecta diagnostic. Unpublished presentation; LLNL-PRES-669264, March 2015.

[11] Melvin L. Tobias. Using the log-normal distribution in analyzing aerosols: The mathematical reasoning underlying the various diameters used an the plotting procedure. Technical Report ORNL/TM-12669, Oak Ridge National Laboratory, 1993.

[12] Klaus Willeke and John E. Brockmann. Extinction coefficients for multimodal atmospheric particle size distributions. *Atmos. Environ.*, 11:995–999, 1977.